High-performance bismuth telluride thermoelectric thin films fabricated by using the two-step single-source thermal evaporation

Ping Fan, Peng-Cheng Zhang, Guang-Xing Liang, Fu Li, Yue-Xing Chen, Jing-Ting Luo, Xiang-Hua Zhang, Shuo Chen, Zhuanghao Zheng

High-performance bismuth telluride thermoelectric thin films fabricated by using the two-step single-source thermal evaporation

Ping Fan [a], Peng-cheng Zhang [a], Guang-xing Liang [a], Fu Li [a], Yue-xing Chen [a], Jing-ting Luo [a], Xiang-hua Zhang [b], Shuo Chen [a], Zhuang-hao Zheng [a, *],

a. Shenzhen Key Laboratory of Advanced Thin Films and Applications, College of Physics and Optoelectronic Engineering, Shenzhen University, Shenzhen, 518060, China.

b. University Rennes, CNRS, ISCR (Institut des Sciences Chimiques de Rennes) – UMR 6226, F-35000 Rennes, France.

* Corresponding Author, Email: zhengzh@szu.edu.cn

Abstract Bismuth telluride (Bi_2Te_3) is an efficient thermoelectric material, and fabricating Bi_2Te_3 thin films with good thermoelectric properties is a prerequisite to realizing the potential of these materials in microdevice application. Controllable content deposition and low-negative thermal treatment are the two main challenges in preparing high-performance thin films. In this study, stoichiometric Bi_2Te_3 thin films were successfully fabricated via the two-step thermal vapor process with a single evaporation source. Then, the rapid thermal process, which could avoid component loss, was used to further improve the crystallinity and thermoelectric properties of thin films. The Seebeck coefficient of Bi_2Te_3 thin films clearly increased after rapid heat treatment, leading to enhanced power factor and good flexibility. Such thin films exhibited low thermal conductivity due to their nano-sized grains, resulting in high ZT of flexible Bi_2Te_3 thin films.

Keywords: Bi_2Te_3 thin film; Thermal evaporation; Two-step process; Single source; Thermoelectric properties

1. Introduction

Given that thermoelectric (TE) materials can directly convert heat energy to electricity, they have great potential application in semiconductor cooling and generator fields [1]. The efficiency of TE materials is related to the dimensionless figure of merit, which is expressed as $ZT = S\sigma T/(\kappa_L + \kappa_e)$, where S is the Seebeck coefficient; σ is the electrical conductivity; T is the absolute temperature; and κ_L and κ_e are the lattice and electrical thermal conductivities, respectively [2]. Several applications have used minimal microwatts of power at high voltages in the operation of mobile electric devices and sensor network systems in the microelectronic industry [3-5]. A TE generator may be an ideal onboard power source in such cases. However, traditional techniques for manufacturing TE materials cannot meet the requirements, such as microsize, lightweight, flexible, and wearable, of these miniaturized devices. Thus, the preparation of TE materials as thin film onto a flexible substrate by using physical or chemical deposition is a promising technology to realize practical microsize and flexible TE materials [6].

Despite the ZT value of more than 2 in various novel TE materials, the classic bismuth telluride (Bi_2Te_3) remains to be an excellent TE material due to its high TE performance at room temperature [7]. The majority of microsize or flexible devices are used commercially at low temperatures. Thus, many studies have investigated the preparation of high-performance Bi_2Te_3 thin films [8-10]. Jin et al. fabricated Bi_2Te_3 thin film with high ZT value and excellent flexibility for highly ordered (000l)-textured nanocrystals on high-quality SWCNT bundles via the sputtering

method [11]. The majority of studies have focused on preparing high-power factor Bi_2Te_3 thin films through the development of thin film growth methods due to the difficulty in the precise measurement of thin film thermal conductivity [12-15].

Thermal evaporation is a promising thin film deposition technique that has also been used in the preparation of Bi_2Te_3 thin films [16-18]. However, controlling the composition content of thin films with a single evaporation source is difficult because Bi and Te have distinctly different evaporation rates. Thus, the coevaporation method is commonly used to prepare Bi_2Te_3 thin films from Bi and Te sources. Rogacheva et al. determined that the preferential growth direction of films prepared by coevaporation was related to the preparation conditions that have a significant effect on the TE properties of thin films [19]. However, the coevaporation method has difficulty in balancing the rate of the two sources and controlling the reaction between different vapor sources that easily leads to impurity phases. Additionally, Bi_2Te_3 thin films prepared at room temperature exhibit poor crystallinity, and high-temperature heat treatment is needed to improve the crystallinity and TE properties [20-22]. However, some Te vacancy defects easily occur in Te-based materials because of its high saturated vapor pressure that will be reevaporated from the grain boundary during heat treatment [23-24]. Some organic materials, such as polyethylene terephthalate and polyimide, have been used as substrates to make the inorganic TE thin films flexible [25]. The majority of these organic materials cannot be used at high temperature for prolonged periods of time. Thus, the traditional annealing process could result in poor flexural mechanical and adhesion properties with the substrate.

In this study, we demonstrate a facile and efficient method for fabricating Bi_2Te_3 thin films by using a single-source physical vapor deposition method. This method is different from the previous dual-source vapor evaporation because the composition of films can be easily controlled by using a two-step evaporation process. Furthermore, rapid thermal processing was used to optimize the TE properties of films to avoid element re-evaporation and flexible substrate damage. Hence, stoichiometric and highly uniform Bi_2Te_3 thin films with good TE properties were successfully fabricated.

2. Experimental

2.1 Material preparation

Bi_2Te_3 powder was synthesized by using the mechanical alloying method. Stoichiometric mixtures of commercial powders Bi (4 N) and Te (4 N) were roughly mixed with a pestle and subjected to mechanical alloying in argon atmosphere. Milling was performed at 450 rpm for 6 hours in a planetary ball mill with a powder-to-ball mass ratio of 1:20. The results show that the prepared powder has a stoichiometric ratio and a single Bi_2Te_3 phase (Fig. S1).

2.2 Film preparation

The prepared Bi_2Te_3 powder was used to fabricate Bi_2Te_3 thin films by using the single-source thermal evaporation method. Polyimide (20 mm × 20 mm × 0.125 mm) was used as the substrate and ultrasonically and sequentially cleaned in acetone, alcohol, and deionized water. Bi_2Te_3 powder (1 g) was placed into a crucible in a high-vacuum chamber with a basic pressure of 1×10^{-3} Pa. The substrate holder was

rotated at a rate of 5 rpm to ensure uniform evaporation. Evaporation current (EVC) was applied from 90 A to 120 A, and the deposition time remained constant for 10 min. Rapid heat treatment (RHT) was used to treat the thin films under vacuum. The target temperature was set to 500 K, and the heat rates were set to 2, 3, 4, and 5 K/s without heat retention.

2.3 Characterization

The phase structures of Bi_2Te_3 thin films were characterized by using X-ray diffraction (XRD; Ultima IV; Rigaku, Japan) in the conventional θ–2θ mode at a scanning rate of 1°/min. The surface morphology and composition of thin films were determined via a scanning electron microscope (SEM, Zeiss Supra 55) with an energy dispersive X-ray microanalysis system and atomic force microscope (AFM, CSPM5500). The film thickness was measured with a Dektak^3 ST surface profile measurement system (Ultima4; Rigaku, Japan). The chemical states of samples were analyzed by using an X-ray photoelectron spectroscope (XPS, Escalab 250Xi) with a monochromatic Al K_α X-ray source with energy of 1486.6 eV. The Seebeck coefficient and electrical conductivity were obtained by using a Seebeck coefficient–electrical conductivity measuring system (SBA458; Netzsch, Germany). Thermal conductivity κ was measured via the Linseis thin film laser flash system (TF-LFA, LINSEIS, Germany) via time-domain thermoreflectance method. A 200 nm-thick Au thin film layer was sputtered on top of the Bi_2Te_3 thin film before the measurement as the transport layer. Carrier concentration and Hall mobility were measured by using the Van der Pauw Hall measurement (HL5500PC, Nanometrics).

3. Results and discussion

Thin films were generally prepared at a certain EVC by using the traditional thermal evaporation method [26]. The prepared Bi_2Te_3 thin film displays enlarged component deviation with the powder due to the different evaporation rates of Bi and Te with a single evaporation source. Such phenomenon is consistent with our experimental results listed in Table S1. Moreover, the films are Te-rich when EVC ≤ 100 A and become Bi-rich after higher currents were used. Thus, the two-step thermal vapor process was used to balance the Bi and Te contents in the thin film. Fig. 1 presents the diagram. The Te-rich layer was first deposited onto the glass substrate at 40 nm with an EVC of 90 A. EVC was increased to 120 A to continue depositing at the Bi-rich layer with thickness of 200 nm. Then, the as-deposited thin films were further treated by using the RHT method. Fig. 2 illustrates the results of the EDS analysis of thin films, in which the as-deposited thin film composition is similar to the atomic ratio of 2:3 (Fig. 2a). Although the RHT condition varied, film composition remained nearly the same (Fig. 2b). The inserted elemental mapping (Sample H2) also shows that Bi and Te are homogeneously distributed without elemental segregation. These results indicate the successful fabrication of the stoichiometric and highly uniform Bi_2Te_3 thin films in this study.

Table 1 shows the room-temperature electrical conductivity σ, Seebeck coefficient S, carrier concentration n, and mobility μ of all the thin films. All samples possess negative S values, thereby indicating the n-type conduction feature, which was consistent with the corresponding bulk materials [27]. For pristine sample H1, $\sigma >$

500.2 S cm^{-1}, which is similar to the value of stoichiometric Bi_2Te_3 thin films [28-30]. However, obtained *S* is extremely low at only −10.1 μV K^{-1}. The poor *S* value is attributed to the very high *n* value, which is approximately two orders of magnitude higher than the optimal range of the Bi_2Te_3 material at ~10^{19} cm^{-1} [31]. The absolute *S* value of films remarkably increase from ~10 μV K^{-1} to over ~100 μV K^{-1} due to the substantial decrease in *n* after heat treatment, and their values are all in the optimal range. By contrast, electrical conductivity is only slightly reduced because of the gradual increase in mobility. Hence, the power factor of films is remarkably enhanced by approximately 10 times compared with that of the as-deposited sample at various RHT conditions. Figs. 3a and 3b show the temperature dependence of σ and *S* of samples H2–H5 in the range of 303−483 K. The σ value of films increases with the increase in temperature that suggests its semiconductor behavior. The absolute *S* value increases to a peak at ~350 K and downshifts at higher temperatures. Fig. 3c presents the calculated power factor $S^2\sigma$ and displays an increasing trend with temperature. Consequently, the film H4 prepared by using the heat rate of 4 K/s has a higher power factor than the others, and the maximum power factor of 0.53 mW m^{-1} K^{-2} is obtained at 478 K. The changes in relative resistance ($\Delta R/R_0$, where ΔR is the difference between the resistance after bending, and R_0 is the origin resistance before bending) of sample H4 were measured to assess the bending flexibility of the thin film with the bending radius about 5 mm (Fig. 3d). The results show that the resistance deviation before and after bending is very small at only ~0.5% within 200 cycles and ~2% after

1000 cycles. This result indicating good flexibility is comparable to the reported results [11, 13].

Analyses were performed to further investigate the underlying factors for the significant changes in the property of the TE thin film because of the minimal differences in film composition. Fig. 4 shows the crystalline structure determined by XRD in the range of 10°–80°. The as-deposited sample obtains the strongest peak at ~27.5°, which belongs to the (015) plane of the Bi_2Te_3 phase. However, many impurity peaks are observed. Given its very high carrier concentration, we deduce that nonregular component defects are formed due to insufficient kinetic energy. This phenomenon results in weak atom migration when thin films are prepared at room temperature despite its stoichiometric composition. By contrast, the films show typical rhombohedral Bi_2Te_3 diffraction peaks after heat treatment, and no impurity peak is observed within the detection limit, thereby indicating the single-crystal structure of the films. Thus, the improved crystallintiy of RHT films remarkably enhances the TE properties. In particular, the peak intensity of the (006) plane evidently increases after heat treatment but only increases slightly when the heat rate is lower than 4 K s^{-1}, and (1010) becomes the strongest plane at 2 K s^{-1}. In many cases, Bi_2Te_3 thin films with (00*l*) have better TE properties than the other films [12, 13]. Thus, the change in the preferred orientation would have caused the different TE properties of the thin films prepared at various RHT conditions. To illustrate the results better, the samples were measured with the AFM, and the images are shown in Fig. 5a, which displays the average surface size of grains. The surface size increases

rapidly when the heat rate decreases from 5 K s^{-1} to 4 K s^{-1}, and further decreasing the heat rate reduces the effect. The Bi_2Te_3 structure consists of Te1–Bi–Te2–Bi–Te1 quintuple layers along the c-direction and are weakly coupled with each other via the van der Waals interactions [31]. This feature structure results in the lower formation energies of (00*l*) plane than those of the others [32]. Therefore, the nuclei gradually merges via heat treatment and preferentially grow to the a(b) direction, thereby causing the increase in the grain surface size. However, a prolonge treatment time will also intensify the atom diffusion across the grain interface and promote nuclear growth along the other orientations.

Fig. 6 shows the high-resolution core-level spectral regions of Bi4f and Te3d for the as-deposited sample and the samples heated at the rates of 2 and 3 K/s. The binding energy of all peaks is corrected by using the C1s energy at 284.4 eV in addition to the charge compensation via the flood gun associated with the spectrometer. Two peaks at energies of ~157 and ~162 eV are observed for all samples in Fig. 6a. These values correspond to the binding energy of $Bi4f_{7/2}$ and $Bi4f_{5/2}$ of single-crystal Bi_2Te_3 [33]. For Te (Fig. 6b), the peaks are obtained at ~572 and ~583 eV, which are also consistent with the data observed from Bi_2Te_3 [33]. The XPS results further prove the successful preparation of intermetallic Bi_2Te_3 compounds. Additionally, the binding energies of Bi4f and Te3d peaks of the as-deposited thin film are slightly larger than that of the single crystal and demonstrate a red shift after RHT. Thus, the XRD results show that certain impurity electron groups may have an effect on the chemical interaction of the Bi-Te bond in

the as-deposited thin film and lead to the higher binding energy of the as-deposited thin film compared with that of pure Bi_2Te_3. The decrease in impurity defects decreases the binding energy of the thin film and becomes closer to that of the single-crystal Bi_2Te_3.

Fig. 7a shows the total thermal conductivity κ_{total} of samples H3 and H4. Lattice thermal conductivity κ_{lat} was also calculated (Fig. 7b) by using the formula $\kappa_{total} = \kappa_{lat} + \kappa_{ele}$, where κ_{ele} is the contribution of electrons. κ_{ele} is estimated via the Wiedemann–Franz law $\kappa_{ele} = L\sigma T$, where the constant L, also known as the Lorenz number, depends on the degree of elasticity in carrier scattering. The temperature dependence of the Lorenz number is calculated, and the results are provided in Table S2 [34]. The films have very low thermal conductivity, which is only ~70% of bulk Bi_2Te_3 [35-38] due to the low lattice thermal conductivity. The AFM images demonstrate that the films have a grain size of ~100 nm. The SEM results also confirm that the films have smooth surfaces and nano-sized particles (see in Fig. S2). Thus, low thermal conductivity is attributed to the nanostructure (Fig. 7c), in which phonons with short wavelengths are effectively scattered by the nano-sized grains, whereas those with long wavelengths are scattered by the grain boundaries with large sizes. Fig. 7d shows the temperature dependence of the ZT value. The estimated maximum ZT values of ~0.47 and ~0.51 are achieved from samples H3 and H4 at ~400 K, respectively. These findings are comparable to the best results of flexible Bi_2Te_3 thin films.

4. Conclusions

Bi_2Te_3 thin films were synthesized with flexible substrates by using the two-step

single-source evaporation method at various rapid heat treatment rates. Stoichiometric Bi_2Te_3 thin films with uniform element distribution were obtained, and the heat rate was crucial in the increase in the Seebeck coefficient. As predicted, the power factor was enhanced by approximately 10 times after RHT. Moreover, the nano-sized grains of thin films resulted in ultralow thermal conductivity, leading to their high ZT values. These findings are comparable to the best value of flexible Bi_2Te_3 thin films. The results demonstrated the efficiency of this innovative technique for the preparation of high-performance flexible thermoelectric thin films.

Acknowledgements

P. Fan, G. X. Liang and F. Li contributed equally. This work is supported by the National Natural Science Foundation of China (Grant No. 11604212), and Shenzhen Key Lab Fund (Grant No. ZDSYS 20170228105421966).

References

[1] J. He, T.M. Tritt, Advances in thermoelectric materials research: Looking back and moving forward, Science, 2017, 357: 1369.

[2] G. J. Snyder, E. S. Toberer, Complex thermoelectric materials, Nat. Mater., 2008, 7: 105-114.

[3] T. Mori, S. Priya, Materials for energy harvesting: At the forefront of a new wave, MRS Bull., 2018, 43: 176-180.

[4] I. Petsagkourakis, K. Tybrandt, X. Crispin, I. Ohkubo, N. Satoh, T. Mori, Thermoelectric materials and applications for energy harvesting power generation, Sci. Tech. Adv. Mater., 2018, 19: 836-862.

[5] C. Dagdeviren, Z. Li, Z. L. Wang, Energy harvesting from the animal/human body for self-powered electronics, Annu. Rev. Biomed. Eng., 2017, 19: 85-108.

[6] Z. Y. Lu, M. Layani, X. X. Zhao, L. P. Tan, T. Sun, S. F. Fan, Q. Y. Yan, S. Magdassi, H. H. Hng, Fabrication of flexible thermoelectric thin film devices by inkjet printing, Small, 2014, 10: 3551.

[7] M. Scheele, N. Oeschler, K. Meier, A. Kornowski, C. Klinke, H. Weller, Synthesis and thermoelectric characterization of Bi_2Te_3 nanoparticles, Adv. Funct. Mater. 2009, 19: 3476-3483.

[8] Z. H. Zheng, P. Fan, J.T. Luo, G.X. Liang, H.L. Ma, X.H. Zhang, C. Yang, Y.Q. Fu, High-performance p-type inorganic–organic hybrid thermoelectric thin films, Nanoscale, 2018, 10: 13511-13519.

[9] Y. Du, K. F. Cai, S. Chen, P. Cizek, T. Lin, Facile preparation and thermoelectric properties of Bi_2Te_3 based alloy nanosheet/PEDOT: PSS composite films, ACS Appl. Mater. Interfaces.2014, 6: 5735-5743.

[10] I. Chowdhury, R. Prasher, K. Lofgreen, G. Chrysler, S. Narasimhan, R. Mahajan, D. Koester, R. Alley, R. Venkatasubramanian, On-chip cooling by superlattice-based thin-film thermoelectrics, Nat. Nanotechnol., 2009, 4: 235.

[11] Q. Jin, S. Jiang, Y. Zhao, D. Wang, J. Qiu, D. M. Tang, J. Tan, D. M. Sun, P. X. Hou, X. Q. Chen, K. P. Tai, N. Gao, C. Liu, H. M. Cheng, X. Jiang, Flexible layer-structured Bi_2Te_3 thermoelectric on a carbon nanotube scaffold, Nat. Mater., 2019, 18: 62-68.

[12] X. Mu, H.u Zhou, D. He, W. Zhao, P. Wei, W. Zhu, X. Nie, H. Liu, Q. Zhang, Enhanced electrical properties of stoichiometric $Bi_{0.5}Sb_{1.5}Te_3$ film with high-crystallinity via layer-by-layer in-situ growth, Nano Energy, 2017, 33: 55-64.

[13] W. Hou, X. Nie, W. Zhao, H. Zhou, X. Mu, W. Zhu, Q. Zhang, Fabrication and excellent performances of $Bi_{0.5}Sb_{1.5}Te_3$/epoxy flexible thermoelectric cooling devices, Nano Energy, 2018, 50: 766-776.

[14] S. J. Kim, J. H. We, B. J. Cho, A wearable thermoelectric generator fabricated on a glass fabric, Energy Environ. Sci., 2014, 7: 1959.

[15] D. Madan, Z. Q. Wang, A. Chen, P. K. Wright, J. W. Evans, High-performance dispenser printed MA p-type $Bi_{0.5}Sb_{1.5}Te_3$ flexible thermoelectric generators for powering wireless sensor networks, ACS Appl. Mater. Interfaces, 2013, 5: 11872.

[16] L. M. Goncalves, C. Couto, P. Alpuim, A. G. Rolo, F. Volklein, J. H. Correia, Optimization of thermoelectric properties on Bi_2Te_3 thin films deposited by thermal co-evaporation, Thin Solid Films, 2010, 518: 2816-2821.

[17] B. Jariwala, D. V. Shah, V. Kheraj, Substrate temperature effect on structural properties of Bi_2Te_3 thin films, J. Nano-Electron. Phys., 2010, 3: 101-105.

[18] L. W. Silva, M. Kaviany, C. Uher, Thermoelectric performance of films in the bismuth–tellurium and antimony–tellurium systems, J. Appl. Phys., 2005, 97: 1.

[19] E. I. Rogachev, A. V. Budnik, M. V. Dobrotvorskay, A.G. Fedorov, S. I. Krivonogov, P. V. Mateychenko, O. N. Nashchekina, A. Y. Sipatov, Growth and structure of thermally evaporated Bi_2Te_3 thin films, Thin Solid Films, 2016, 612: 128-134.

[20] Y. Deng, H. Liang, Y.Wang, Z. Zhang, M. Tan, J. Cui, Growth and transport properties of oriented bismuth telluride films, J. Alloys Compd., 2011, 509: 5683-5687.

[21] P. H. Le, C. N. Liao, C. W. Luo, J. Leu, Thermoelectric properties of nanostructured bismuth-telluride thin films grown using pulsed laser deposition, J. Alloy. Compd., 2014, 615: 546-552.

[22] N. Peranio, M. Winkler, M. Durrschnabel, J. Konig, O. Eibl, Assessing antisite defect and impurity concentrations in Bi_2Te_3 based thin films by high-accuracy chemical analysis, Adv. Funct. Mater., 2013, 23: 4969-4976.

[23] C. Sudarshan, S. Jayakumar, K. Vaideki. C. Sudakar. Effect of vacuum annealing on structural, electrical and thermal properties of e-beam evaporated Bi_2Te_3 thin films, Thin Solid Films, 2017, 629: 28-38

[24] D. Takemori, M. Okuhata, M. Takashiri, Thermoelectric properties of electrodeposited bismuth telluride thin films by thermal annealing and homogeneous electron beam irradiation, ECS Trans, 2017, 75: 123-131.

[25] W. Zhu, Y. Deng, L. Cao, Light-concentrated solar generator and sensor based on flexible thin-film thermoelectric device, Nano Energy, 2017, 34: 463-471.

[26] J. Numus, H. Bottner, H. Beyer, A. Lambrecht, Epitaxial bismuth telluride layers grown on (111) barium fluoride substrates suitable for MQW-growth, 18th International Conference on Thermoelectrics 2000, 696.

[27] C. Zhang, X. A. Fan, J. Hu, C. Jiang, Q. Xiang, G. Li, Y. Li, Z. He, Changing the band gaps by controlling the distribution of initial particle size to improve the power factor of n–type Bi_2Te_3 based polycrystalline bulks, Adv Eng Mater, 2017.

[28] J. Krumrain, G. Mussler, S. Borisova, T. Stoica, L. Plucinski, C. M. Schneider, D. Grutzmacher, MBE growth optimization of topological insulator Bi_2Te_3 films, J. Cryst. Growth, 2011, 324:115.

[29] A. Giani, F. Pascal-Delannoy, A. Boyer, A. Foucaran, M. Gschwind, P. Ancey, Elaboration of Bi_2Te_3 by metal organic chemical vapor deposition, Thin Solid Films, 1997, 303:1-2.

[30] A. Dauscher, A. Thomy, H. Scherrer, Pulsed laser deposition of Bi2Te3 thin films, Thin Solid Films 280 (1996) 61,

[31] F. Hao, T. Xing, P. Qiu, P. Hu, T. Wei, D. Ren, Xun Shi, L. Chen, Enhanced Thermoelectric Performance in n‑Type Bi_2Te_3‑Based Alloys via Suppressing Intrinsic Excitation, ACS Appl. Mater. Interfaces 2018, 10, 21372-21380.

[32] D. Kong, W. Zhu, Z. Guo, Y. Deng, High-performance flexible Bi_2Te_3 films based wearable thermoelectric generator for energy harvesting, Energy, 2019, 175: 292-299.

[33] P. Kumar, P. Srivastava, J. Sing3, R. Belwal, M. K. Pandey, K. S. Hui, K. N. Hui, K. Singh, Morphological evolution and structural characterization of bismuth telluride (Bi_2Te_3) nanostructures, J. Phy. D Appl. Phy., 2013, 46: 285301.

[34] L. Yong, L. D. Zhao, Y. C. Liu, J. L. Lan, X. Wei, L. Fu, B. P. Zhang, D. Berardan, N. Dragoe, Y. H. Lin, C. W. Nan, J. F. Li, H. M. Zhu, J. Am. Chem. Soc. 2011, 133, 20112.

[35] X. B. Zhao, X. H. Ji, Y. H. Zhang, T. J. Zhu, J. P. Tu, X. B. Zhang, Bismuth telluride nanotubes and the effects on the thermoelectric properties of nanotube-containing nanocomposites, Appl. Phys. Lett., 2005, 86: 062111.

[36] W. Xie, X. Tang, Y. Yan, Q. Zhang, T. M. Tritt, Unique nanostructures and enhanced thermoelectric performance of melt-spun BiSbTe alloys, Appl. Phys. Lett., 2009, 94:102111.

[37] J. J. Shen, T. J. Zhu, X. B. Zhao, S. N. Zhang, S. H. Yang, Z. Z. Yin, Recrystallization induced in situ nanostructures in bulk bismuth antimony tellurides: A simple top down route and improved thermoelectric, Energy Environ. Sci., 2010, 3: 1519-1523.

[38] L. Hu, H. Wu, T. Zhu, C. Fu, J. He, P.Ying, X. Zhao, Tuning multiscale microstructures to enhance thermoelectric performance of n-type bismuth-telluride-based solid solutions. Adv. Energy Mater. 2015, 5, 1500411.

Table 1Thermoelectric properties of thin films at room temperature

Sample	Heating rate (Ks^{-1})	σ (Scm^{-1})	S ($-\mu VK^{-1}$)	PF ($mWm^{-1}K^{-2}$)	n (cm^{-3})	μ ($cm^2V^{-1}s^{-1}$)
H1	As-deposited	500.2	-10.1	0.005	1.41×10^{21}	2.17
H2	2	257.1	-128.4	0.424	4.39×10^{19}	39.4
H3	3	262.9	-125.9	0.416	4.61×10^{19}	38.7
H4	4	280.9	-125.7	0.444	4.80×10^{19}	34.7
H5	5	305.2	-118.8	0.431	5.03×10^{19}	32.3

Figure Captions

Figure 1 Schematic of the preparation of thin films

Figure 2 (a) EDS test results of the as-deposited thin film and (b) atomic composition of thin films (inset: elemental mapping of sample H2)

Figure 3 Temperature dependence of thin films after heat treatment: (a) electrical conductivity, (b) Seebeck coefficient, and (c) power factor; (d) bending test of sample H4

Figure 4 Powder X-ray diffraction of all thin films

Figure 5 AFM images of thin films after heat treatment

Figure 6 Binding energy obtained from the high-resolution core-level spectral regions of (a) Bi4f and Te3d of the as-deposited sample and the samples prepared at heat rates of 1 and 3 Ks^{-1}.

Figure 7 (a) Total thermal conductivity and (b) the calculated lattice thermal conductivity of samples H3 and H4 as a function of temperature, (c) various phonon scattering mechanisms via the nanostructure and grain boundary defect, and (d) temperature dependence of the ZT value.

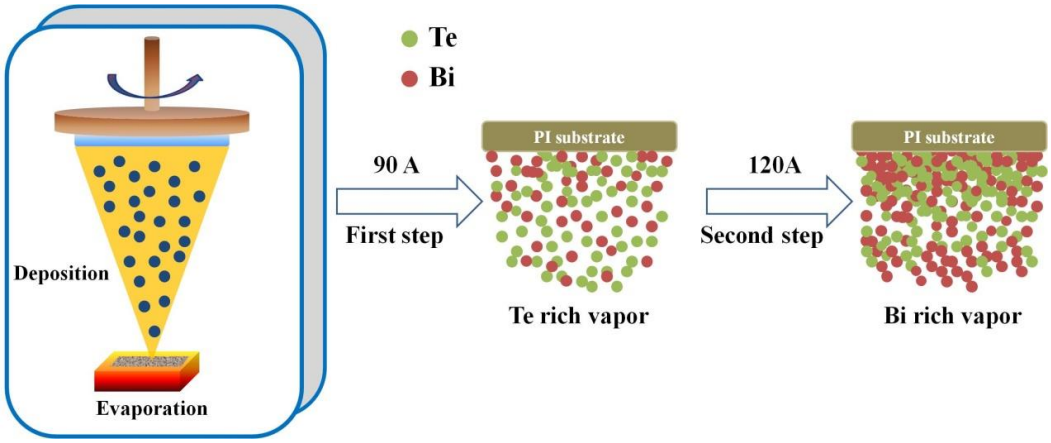

Figure 1

(a)

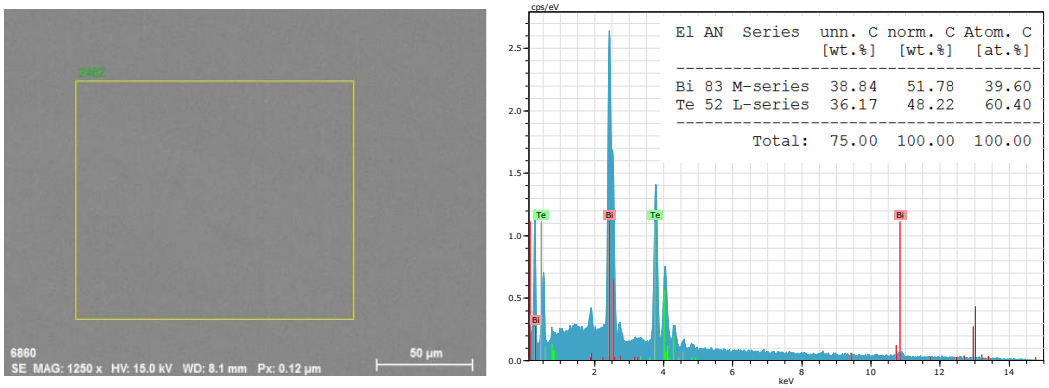

(b)

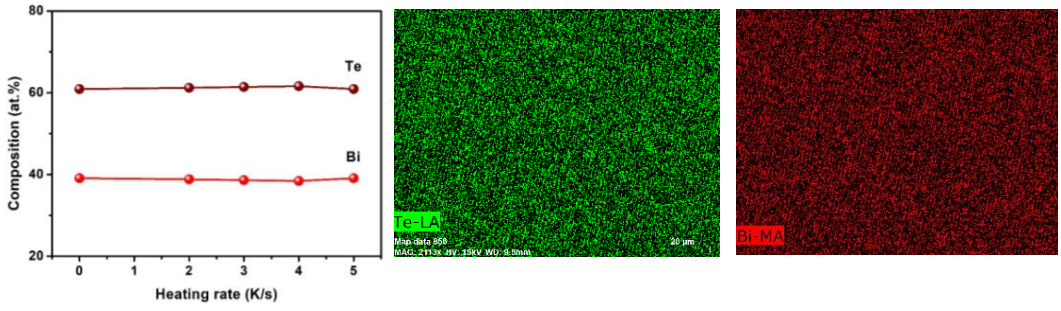

Figure 2

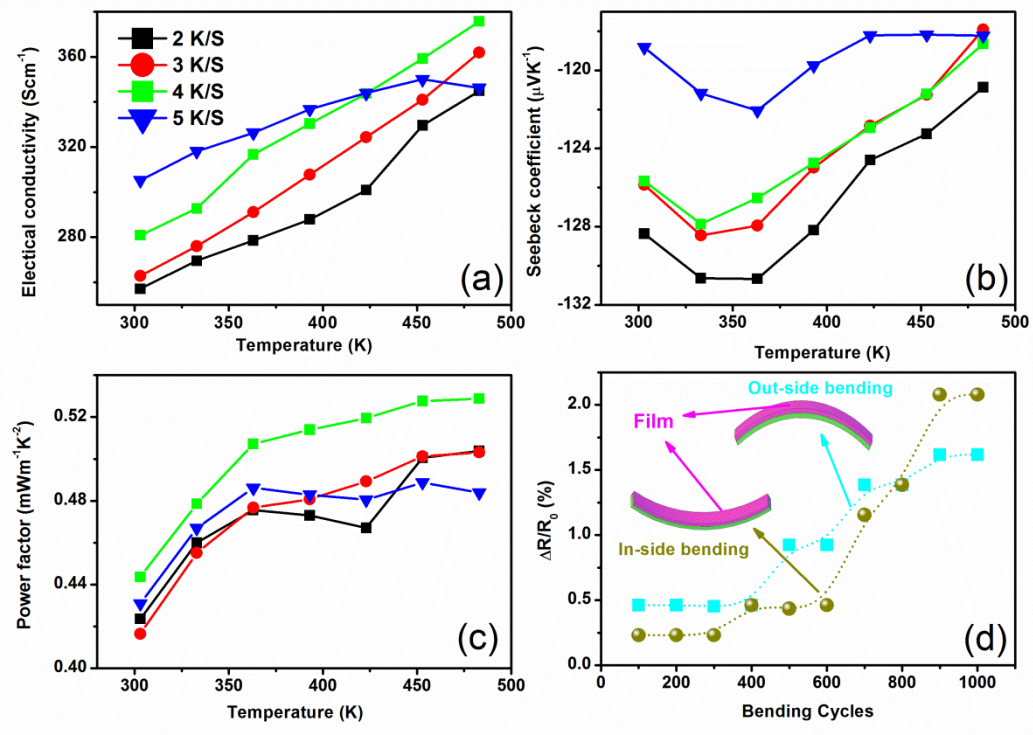

Figure 3

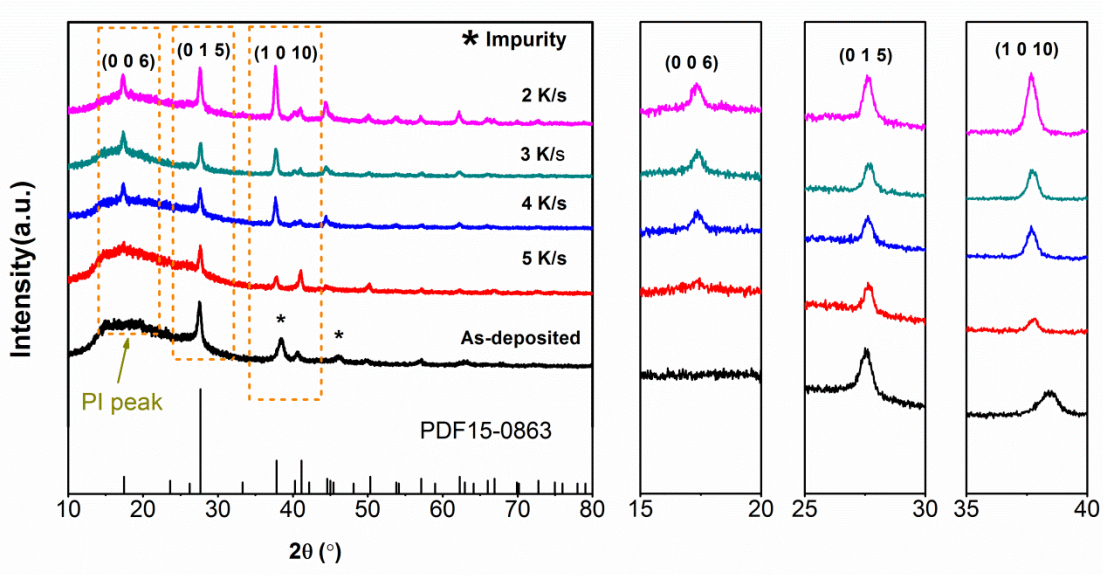

Figure 4

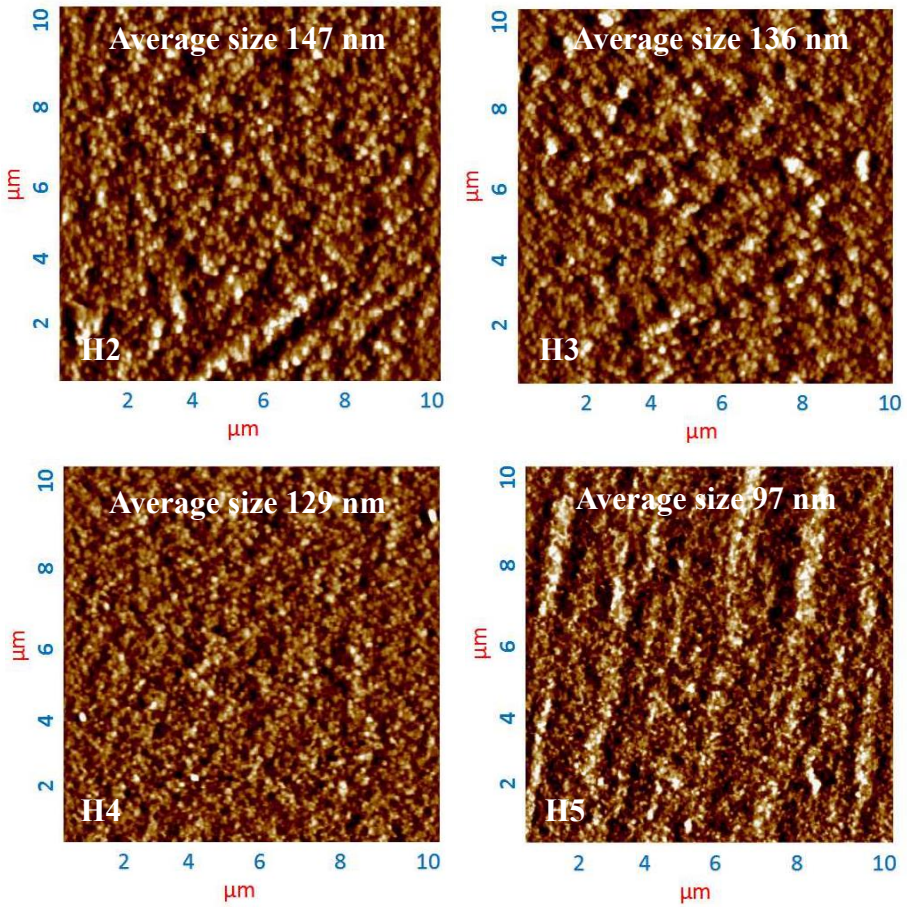

Figure 5

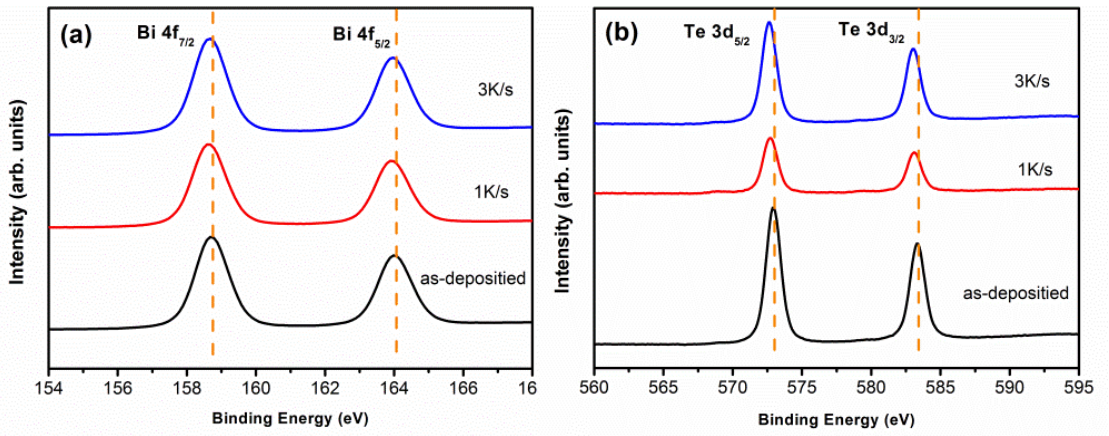

Figure 6

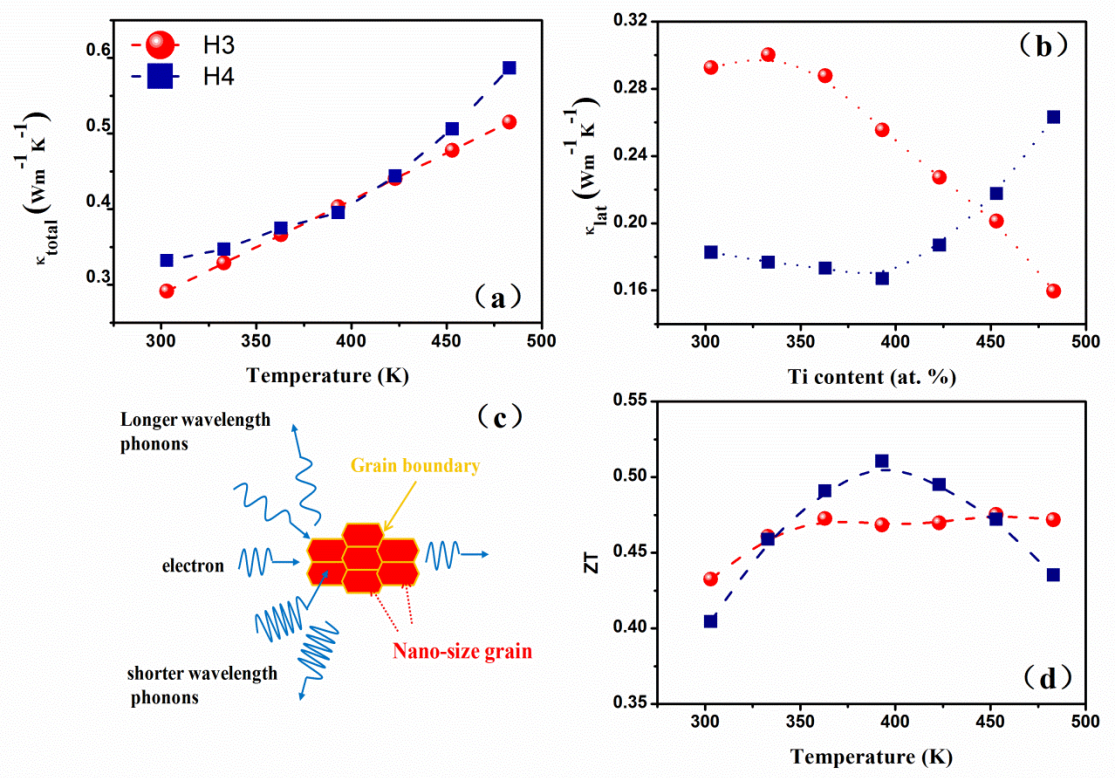
H3
H4
(a)
Temperature (K)
(b)
Ti content (at. %)
(c)
Longer wavelength phonons
Grain boundary
electron
Nano-size grain
shorter wavelength phonons
(d)
ZT
Temperature (K)

Figure 7